17th World Conference on Earthquake Engineering, 17WCEE
Sendai, Japan - September 13th to 18th 2020

Effect of Forward Directivity and Non-forward directivity ground motions on the Inter-story isolation system.

A. Saha[(1)], S.K. Mishra[(2)]

[(1)] *Research Scholar, IIT Kanpur,arijitsa@iitk.ac.in*
[(2)] *Associate Professor, IIT Kanpur, smishra @iitk.ac.in*
…

Abstract

Inter-story isolation is proposed for seismic vibration control of building. The performance of (High Damping Rubber Bearing) HDRB based inter-story isolation is investigated under near- fault motions, especially pulse type motions. Ground motions due to forward directivity (FD) and motions from non-forward directivity (NFD) are consider. Two different structural system designed in accordance with the Eurocode are subjected to a suite of twenty-five FD motions and twenty-five non-FD motions, binned into DBE (Design Basis earthquake) and MCE (Maximum Considered Earthquake) hazard levels. Further stiffening at large displacement of HDRB is incorporated in the analysis to adequately consider the influence of the amplified displacement demands subjected to long period pulse(s). Nonlinear dynamic analysis reveals that, the FD ground motions impose significantly larger demand (story displacement, drift, absolute acceleration and residual drift) compared to the non-FD motions. The effects of pulse characteristics are demonstrated by adopting a mathematical pulse model, that facilitates manipulation of the pulse characteristics. The effect of structural non-linearity is also demonstrated.

Keywords: Near-fault ground motions, Inter-story isolation system,High-damping rubber bearing Non-linear dynamic analysis

1. Introduction

Base isolation (BI) based seismic vibration control strategy developed enormously for the seismic protection of the structure from the damaging effect of an earthquake. Another vibration control strategy, Tuned mass damper (TMD) is implemented by attaching a small mass to the main structure for controlling the structural responses subjected to wind-induced vibration. However, the effectiveness of the BI system is questionable for tall flexural building subjected to near-fault ground motions. An Inter-story isolation (ISI) system has been proposed by several researchers [1-2] to overcome the above issue. Ziyaeifar and Noguchi [3] conducted a dynamic analysis of tall flexural partial mass isolated (PMI) building. They conclude that PMI technique is effective in reducing the seismic response of tall structures. Charmpis et al. [4] conducted an optimization study of the ISI system to minimize the maximum floor acceleration with specified constraints such as inter story drift, base displacement and isolator cost. Reggio and Angelis [5] proposed an optimal design methodology of the inter-story isolated system subjected to maximizing the energy dissipation index (EDP). Dynamic characteristics of the inter-story isolation system and seismic responses of three degrees reduced order model have been carried out by Wang et. al [6].

In the current study, an effort has been to check the efficacy of the ISI system under near- fault pulse and non-pulse ground motions. An extensive non-linear dynamic analysis is carried out for four mid to high-rise steel moment-resisting frame designed according to the Eurocode (EC8). The input ground motions are scaled into two hazard bins such as, design basis earthquake (DBE) and maximum considered earthquake (MCE). In the present analysis, High damping rubber bearing (HDRB) with non-linear behavior (shows stiffening effect) is incorporated. The results obtained from the response histories analysis are presented in terms of the log-normal statistics such as, peak floor displacement, peak inter-story drift ratio and peak absolute floor acceleration normalized by peak ground acceleration. Lastly, the effect of structural non-linearity (both in the upper story and in lower story block) on the response control behavior is demonstrated by contrasting with the respective linear behavior of structures.

2. Structural configuration

In the present study 15th stories steel moment resisting frame (SMRF) is selected from a study reported by [7]. The section details of the SMRF are reported in Table 1 and the frame was designed based on the in Eurocode 3 (EC3-1992) [8] and Eurocode 8 (EC8-2004) [9]. The gravity loads on the beam are considered as 27.5 kN/m. The inelastic force deformation behavior of the member is taken into account by assigning a plastic hinge at the end of each member. The properties of the plastic hinges are assigned as suggested by FEMA 356 (2000) [10]. The inherent viscous damping ratio of the structure is considered as 3% in the first and second mode. The first (T_1) and second (T_2) modal period of the structure comes out to be 2.22 and 0.75 second, respectively. The yield acceleration capacity $\left(a_y\right)$ of the structure is obtained from a push over analysis. The Inter-story isolation structure are realized by placing the isolation bearing in between the story, such as above 9th and 12th story. The ISI structures are denoted as B(9,6) and B(12,3), in which first and second number refers to the number of story in lower structure block (LSB) and upper structure block (USB), respectively.

Table 1 Beam and column section details of the structure

Frame	**Section details** **column (HEB)-beam (IPE)**	a_{cv}	**T_1**	**T**	**a_y**
B	550-300 (1)+550-400 (2-3)+550-450 (4-5)+500-400 (6-7)+450-400 (8-12)+450-360 (13-14)+450-330 (15)	3.95	2.22	0.75	0.12

3. Ground motions selection and scaling

The results of non-linear dynamic analysis largely depends on the characteristics of the ground motions. This is due to the wide variation of the frequency, amplitude and ground motion duration, which are varies from one record to another ground motion record. Thereby, the selection of the ground motions are essential for the structural assessment. In the present study, a suite of near-fault pulse and non-pulse ground motions are considered for the detailed analysis. The pulse ground motions are selected from the database provided by Baker et. al [11]

These motions (pulse and non-pulse) are scaled into two hazard levels such as, design basis earthquake (DBE) and maximum considered earthquake (MCE). These ground motions are categorized based on the peak ground velocity to peak ground acceleration ratio (PGV/PGA). It shows that, average PGA values for pulse and non-pulse ground motions are 0.33g and 0.41g. On the other hand there average PGV values are (79.3 cm/s and 38.6 cm/s for pulse and non-pulse motions, respectively. However, the scaling of ground motions is necessary to evaluate their potential effect on structural damage. In the present analysis, ground motions are scaled to match the target spectral ordinate at the fundamental period of each fixed based structure in the design spectrum provided by Eurocode 8 [EC8] of type I and soil class B [9]. The design ground acceleration is selected in such a way that, structure experiences nonlinear deformation (beyond yield acceleration). The considered design basis earthquake (DBE) and maximum considered earthquake (MCE) are equal to 0.35g and 0.52g (1.5*DBE), respectively.

4. Equation of motion

Consider a typical multi degree of freedom (DOF) shear building structure. Let N_l and N_u are the degrees of freedom of the lower and upper structure respectively. The governing equation of motion for the upper structure can be expressed as,

$$[M_u]\{\ddot{x}_u\}+[C_u]\{\dot{x}_u\}+f_S(x_u,\dot{x}_u)=-[M_u]\{r_u\}\left\{\ddot{x}_g+\ddot{x}_l^n+\ddot{x}_b\right\} \tag{1}$$

In which $[M_u]$ and $[C_u]$ are the mass and damping matrix of the upper structure of size $(N_u \times N_u)$. $f_S(x_u,\dot{x}_u)$ is the non-linear force behavior of the upper structure column. $\{\ddot{x}_u\}$, $\{\dot{x}_u\}$ and $\{x_u\}$ are the lateral floor displacement vector $(N_u \times 1)$ of the upper structure relative to the bearing. $\{r_u\}$ is the influence coefficient vector containing $\{1,1,1,.....,1\}^T$ of size $(N_u \times 1)$. $\ddot{x}_l^n$ and $\ddot{x}_b$ are the acceleration of the lower structure at (N_l)DOF respect to the ground level and acceleration of the isolation mass (m_b) respect to the lower structure (N_l) DOF. $\ddot{x}_g$ is the ground acceleration. The governing equation of motion for the bearing mass is expressed as,

$$m_b\ddot{x}_b+F_b\left(x_b,\dot{x}_b\right)-C_1^u\dot{x}_1^u-K_1^u x_1^u=-m_b\left(\ddot{x}_l^N+\ddot{x}_g\right) \tag{2}$$

where (m_b) is the mass at the bearing level. $F_b\left(x_b,\dot{x}_b\right)$ is the restoring force of the HDRB. C_1^u and K_1^u are the damping and stiffness of the first story of the upper structure, respectively.

The governing equation of motion of the lower structure can be written as,

$$[M_l]\{\ddot{x}_l\}+[C_l]\{\dot{x}_i\}+f_S(x_l,\dot{x}_l)-\begin{Bmatrix}F_b\left(x_b,\dot{x}_b\right)\\ \{0\}_{\left(N_l-1\times 1\right)}\end{Bmatrix}=-[M_l]\{r_l\}\{\ddot{x}_g\} \tag{3}$$

In which $[M_l]$ and $[C_l]$ are the mass and damping matrix of the upper structure of size $(N_l \times N_l)$. $\{\ddot{x}_l\}$, $\{\dot{x}_l\}$ and $\{xl\}$ are the lateral floor displacement vector $(N_l \times 1)$ of the upper structure relative to the bearing. $f_S(x_l, \dot{x}_l)$ is the non-linear force behavior of the lower structure column. $\{\eta\}$ is the influence coefficient vector containing $\{1,1,1,.....,1\}^T$ of size $(N_l \times 1)$.

5. Non-linear modeling of High Damping Rubber Bearing (HDRB)

In the present study, high damping rubber bearings isolation system is employed for the non-linear dynamic analysis. HDRB exhibit higher stiffness and damping at low shear strain as well as higher strain, which is advantageous for serviceability and major earthquake scenario. However, damping of the HDRB may be increased by adding extra-fine carbon filler, oil and resins. Extensive numerical analysis of the Inter-story isolated system requires a simple and accurate equivalent model of the HDRBs. Thereby analysis can be completed within a reasonable time. The Bouc-Wen model can accurately capture the behavior of the HDRBs at low to moderate shear strain. However, this model is unable to capture the nonlinear stiffening behavior at high strain. Thereby, from the particular point of view, mechanical behavior of the bearing is established by connected the multi-linear elastic and elastic perfectly plastic hysteretic element or Bouc-Wen model in parallel combination.

The force deformation behavior of the multilinear elastic spring is denoted by the following relationship [12],

$$F_s(u) = \begin{cases} k_1 u & ; \quad u \le u_1 \\ \dfrac{(k_2 - k_1)(u - u_1)^2}{2(u_2 - u_1)} sign(u) + k_1 u & ; \quad u_1 < u \le u_2 \\ \dfrac{(k_2 - k_1)(u_1 + u_2)}{2} sign(u) + k_2 u & ; \quad u > u_2 \end{cases} \tag{4}$$

Where k_1 and k_2 denotes the stiffness of the multi-linear link element corresponds to the design limits u_1 and u_2, described in Figure. The $sign(u)$ function is defined as,

$$sign(u) = \begin{cases} 1 & if \quad u > 0 \\ 0 & if \quad u = 0 \\ -1 & if \quad u < 0 \end{cases} \tag{5}$$

The force deformation behavior of the elastic perfectly plastic hysteretic element or Bouc-Wen model (post to pre yield stiffness ratio α =0) is denoted by the following relationship,

$$F_z = F_y Z \tag{6}$$

Where Z is the non-dimensional hysteretic parameter. The evolution of the variable Z is expressed in a differential form [13]

$$\frac{dZ}{dt} = \begin{cases} \left(\dfrac{\bar{k}}{F_y}\right)\dfrac{du}{dt}\left(1 - |Z|^n\right) & if \quad Z\dfrac{du}{dt} > 0 \\ \left(\dfrac{\bar{k}}{F_y}\right)\dfrac{du}{dt} & otherwise \end{cases} \tag{7}$$

It may be interpreted that yield force F_y is directly proportional to the effective damping of the bearing and expressed by the following equation,

$$F_y = \frac{\pi\beta k_1 u}{(2-\pi\beta)} \tag{8}$$

The combined force-deformation behavior of the Bearing is denoted as,

$$F(u) = F_s(u) + F_z(u,\dot{u}) \tag{9}$$

The main design parameters of the bearing are Isolation period (T), effective damping (β), yield force (Q), displacement limits (u_1, u_2, u_y), thickness of the rubber (H), initial stiffness (K_{in}), post yield stiffness (K_1) and higher stiffness (K_2) beyond displacement limit (u_2).

The isolation period (T) of the bearing is selected based on the post yield stiffness regime by considering superstructures assumed to be rigid behavior. The post yield (K_1) stiffness of the isolation system is represented by the following expression,

$$\alpha k = (2\pi / T)^2 (W / g) \tag{10}$$

Where W is the weight over each isolation bearing and g is the acceleration due to gravity.

To find out the compatibility of the mathematical model experimental study has been carried out on a scaled specimen subjected to the pressure of 10 MPa and frequency of 0.5 Hz. Corresponding characteristics displacement limits of the mathematical model are related to the thickness of the rubber (H),

$$u_1 = 1.2H, \quad u_2 = 1.3H, \quad u_y = 0.07H \tag{11}$$

The initial (k_1) and hardening stiffness (k_2) of the bearing can be expressed through the following relationship, $k_{in} = F_y / u_y \quad k_2 = 2k_1$.

The HDRBs are installed in the particular stories, pertaining to the specific structural configuration. The first and second numbers in the brackets ( ) are the number of stories in lower and upper blocks, respectively. The corresponding configuration are listed in Table 2. The total rubber thickness of the bearing is considered as 35 cm. Notation for the HDRB bearings are as follows, HDRB-A ($(T = 3\text{sec}, \beta = 10\%)$, HDRB-B $(T = 3\text{sec}, \beta = 20\%)$, HDRB-C $(T = 4\text{sec}, \beta = 10\%)$ and HDRB-D $(T = 4\text{sec}, \beta = 20\%)$. The schematic diagram of the ISI structure and HDRB bearing are shown in Figure 1.

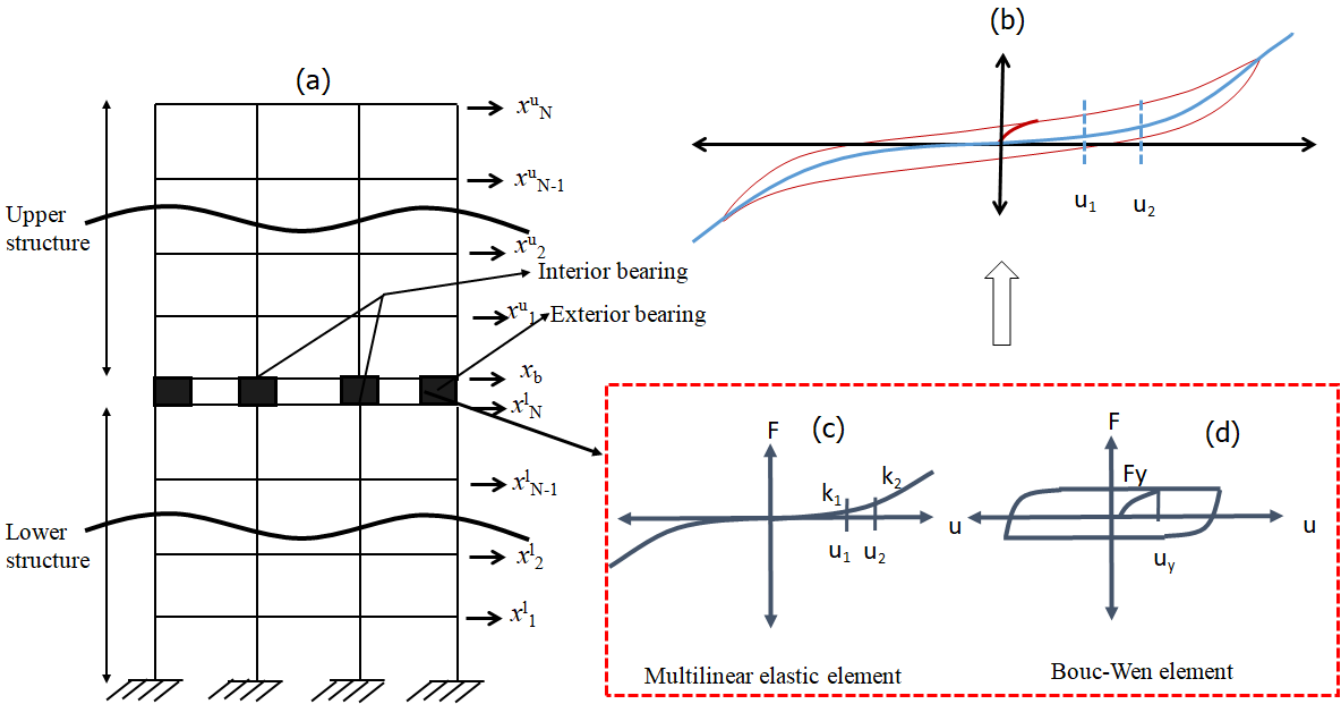

Figure 1 Schematic diagram of (a) ISI frame, (b) force deformation behavior of the HDRB, and modelling of the (c) multi-linear elastic link element and (d) Bouc-Wen element.

Table 2 Bearing properties adopted for the Inter-story isolated (ISI) system

Frame	(USB/LSB)	T s	β In Percent	Initial stiffness of elasto-plastic element $(\bar{k})$ in kN/m		Post yield stiffness $(\alpha\bar{k})$ kN/m		Further hardening stiffness (k_2) in kN/m		Yield force (F_y) in kN	
				exterior	interior	exterior	interior	exterior	interior	exterior	interior
B	(12, 3)	3	10	348.87	687.85	131.12	258.51	262.25	517.03	8.54	16.85
			20	857.43	1690.43	131.12	258.51	262.25	517.03	21.00	41.41
		4	10	196.24	386.89	73.75	145.41	147.51	290.83	4.80	9.47
			20	482.30	950.87	73.75	145.41	147.51	290.83	11.81	23.29
B	(9,6)	3	10	626.44	1200.49	235.45	451.21	470.90	902.43	15.35	29.41
			20	1539.62	2950.47	235.45	451.21	470.90	902.43	37.72	72.28
		4	10	352.37	675.27	132.44	253.80	264.88	507.61	8.63	16.54
			20	866.03	1659.64	132.44	253.80	264.88	507.61	21.21	40.66

6. Results and Discussion

The present section demonstrates the detailed assessment of inter-story isolated system for each structural configuration subjected to the listed near-fault pulse and non-pulse type ground motions, which helps to assess the importance of various response parameters. The responses of interest are peak relative floor displacement (PFD), peak inter-story drift (IDR) and peak horizontal floor acceleration normalized respect to peak ground acceleration (PHFA/PGA). PFD and IDR are important response parameters in terms of the displacement- based design of the structure and damage associated with the structural elements. Although IDR is the straightforward estimate of the damage associated with the drift sensitive non-structural components (partition wall). However, PHFA governs the transmission of forces to a structure, which affect the performance of non-structural components.

Distribution of the peak responses are assumed to follow lognormal distribution $\left(\overline{X}\right)$ [1] and dispersion of the responses is estimated through lognormal standard deviation $\left(\sigma_X\right)$.

$$\overline{X} = \exp\left(\sum_{i=1}^{n} \ln X_i / n\right) \tag{12}$$

$$\sigma_X = \sqrt{\left(\sum_{i=1}^{n} (\ln X_i - \ln \overline{X})^2 / n - 1\right)} \tag{13}$$

Where n is the number of ground motions pertaining to each hazard level. Symbol X_i refers to the desired peak response from time history analysis subjected to i-th motion. The statistics of the response are expressed in terms of 16^{th} , 50^{th} (median) and 84^{th} percentile values as,

$$\left(X^{16}\right) = \overline{X}e^{-\sigma X} \qquad \left(X^{84}\right) = \overline{X}e^{\sigma X} \tag{14}$$

Story wise variation of peak floor displacement (PFD) response of each ISI configuration system are shown in Figure 2. The first and second row in each figure denotes the median response for pulse and non-pulse ground motions under DBE and MCE hazard bins. It can be observed that lower structure experiences relatively much lesser displacement compared to the fixed base structure. However, reduction efficiency is much higher for non-pulse ground motions as compared to the pulse ground motions. It may be noted that, bearing displacement attained much higher in pulse ground motions as compared to the non-pulse ground motions. Story wise variation of peak inter-story drift (%) response of each ISI configuration system are shown in Figure 3. It may be noted that, increasing ISI structure B(9,6) mass ratio (upper structure to lower structure mass), reduction in IDR response is higher as compared to the lower mass ratio ISI system B(12,3). Story wise variation of peak absolute floor acceleration response (PHFA) of each ISI configuration system are shown in Figure 4. Towards better understanding acceleration amplification factor is evaluated for all fixed base and ISI system. In this study acceleration amplification factor is defined as ratio of peak floor acceleration (PFA) to peak ground acceleration (PGA). It has been observed from the Figure 4 that, response reduction efficiency is much higher for non-pulse ground motion as compared to the pulse ground motions.

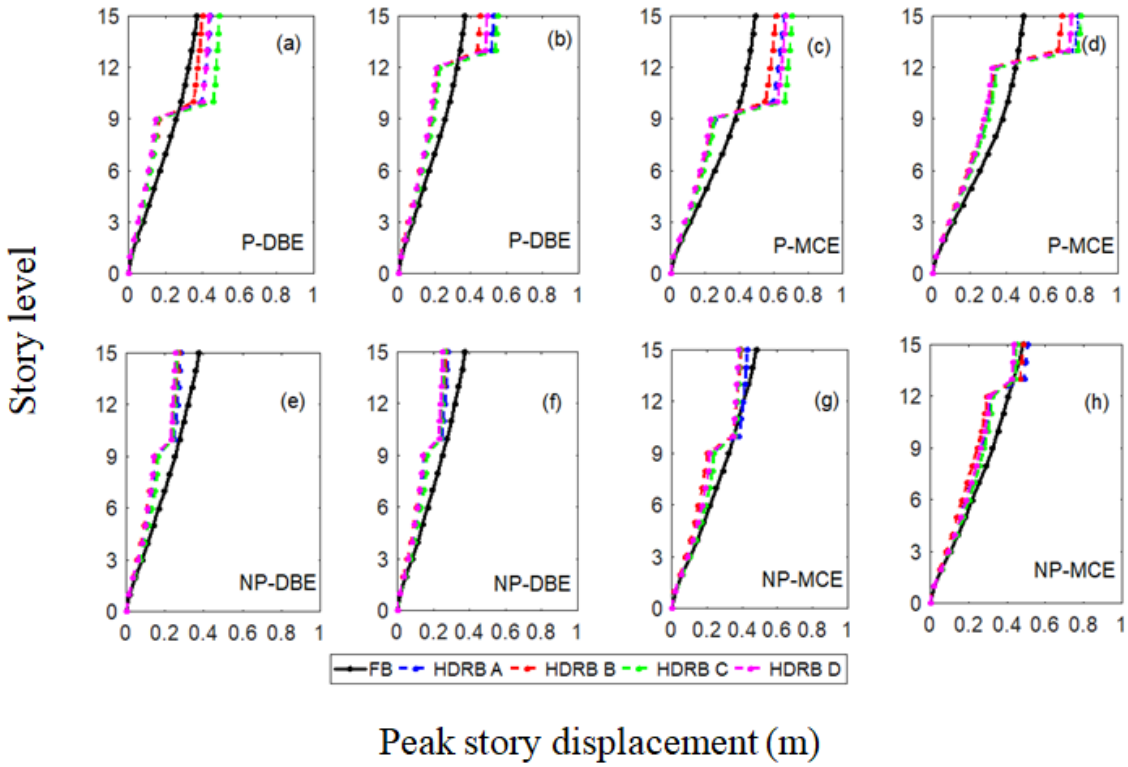

Figure 2 Median relative floor displacement of inter-story isolated system subjected to pulse type DBE hazard for (a) B(9,6), (b) B(12,3), subjected to MCE hazard for (c) B(9,6), (d) B(12,3). Similar response for non-pulse type DBE hazard for (e) B(9,6), (f) B(12,3), subjected to MCE hazard for (g) B(9,6), (h) B(12,3).

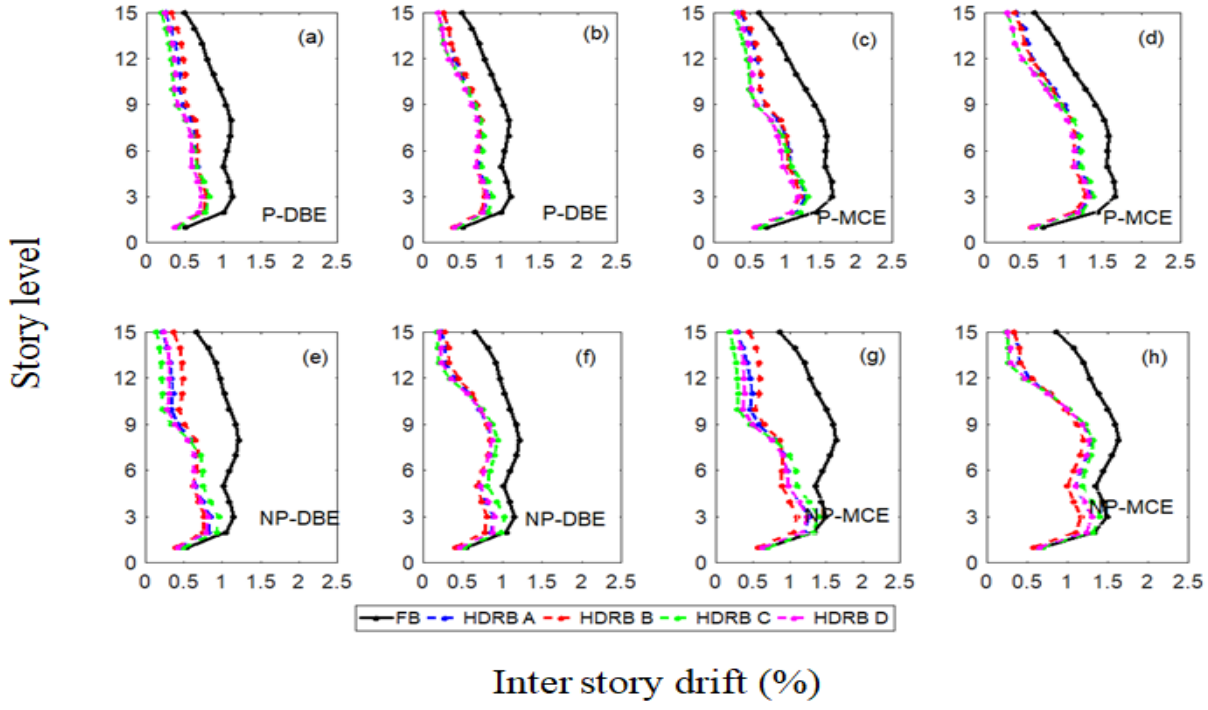

Figure 3 Median inter-story drift ratio (%) of inter-story isolated system subjected to pulse type DBE hazard for (a) B(9,6), (b) B(12,3), subjected to MCE hazard for (c) B(9,6), (d) B(12,3). Similar response for non-pulse type DBE hazard for (e) B(9,6), (f) B(12,3), subjected to MCE hazard for (g) B(9,6), (h) B(12,3).

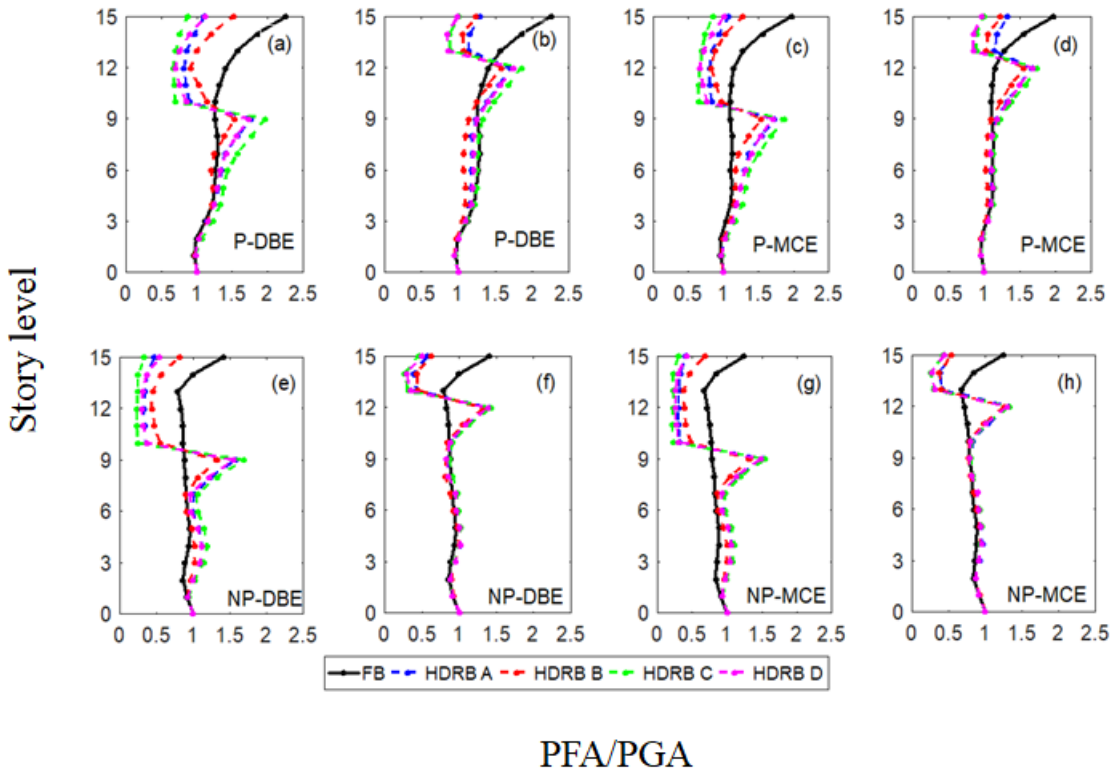

Figure 4 Median acceleration amplification factor of inter-story isolated system subjected to pulse type DBE hazard for (a) B(9,6), (b) B(12,3), subjected to MCE hazard for (c) B(9,6), (d) B(12,3). Similar response for non-pulse type DBE hazard for (e) B(9,6), (f) B(12,3), subjected to MCE hazard for (g) B(9,6), (h) B(12,3).

7. Sensitivity analysis of the ISI system subjected to a simplified mathematical pulse model.

In this section the ISI systems are re-analyzed subjected to simplified mathematical pulse model. For simulating the near fault pulse type ground motion within 20 km from the fault site, the mathematical pulse model proposed by Mavroeidis and Papageorgiou (MP) is considered herein [14]. The velocity time history of the MP pulse model is the product of harmonic oscillator and a symmetric bell-shaped function and can be expressed as,

$$v(t)=\begin{cases}\frac{A}{2}[1+\cos(\frac{2\pi f_p}{\gamma}(t-t_0))]\cos[2\pi f_p(t-t_0)+v], & t_0-\frac{\gamma}{2f_p}\le t\le t_0+\frac{\gamma}{2f_p} \quad with \quad \gamma>1\\ 0, & otherwise\end{cases} \tag{15}$$

The acceleration time history is obtained by integral transformation of velocity and expression as,

$$a(t)=\begin{cases}-\frac{A\pi f_p}{2}[\sin(\frac{2\pi f_p}{\gamma}(t-t_0))\cos[2\pi f_p(t-t_0)+v]+\gamma\sin[2\pi f_p(t-t_0)+v]\left[1+\cos(\frac{2\pi f_p}{\gamma}(t-t_0))\right] & \\ 0, \quad otherwise & \end{cases} \tag{16}$$

$$t_0-\frac{\gamma}{2f_p}\le t\le t_0+\frac{\gamma}{2f_p} \quad with \quad \gamma>1$$

Where (A) is the amplitude of the velocity pulse, f_p is the prevailing frequency of the pulse, γ is controlling oscillator character (number of zero crossing) of the pulse, v denotes the phase angle of the amplitude modulated harmonic, t and t_0 defines time and epoch of the envelopes peak. The pulse period (T_p) of the signal is defined as inverse of the prevailing frequency (f_p).

In this section, a parametric investigation is carried out to establish relationship between pulse period of the MP pulse period and maximum inter-story drift ratio (MIDR %) of the two ISI structure considered herein B(9,6) and B(12,3). The influence of pulse period on the IDR response is shown in Figure 5. For this purpose acceleration pulses are generated with following parameters, A=100 cm/sec, $v = 90°$, $\gamma = 1.5$ and $T_p = [0.5 - 7]$ sec with an increment of 0.25. It is observed from the Figure 5 that MIDR response as a function of (T_p) shows two distinct peak (indicating resonance occurs) corresponds to the first and second modal period of the ISI system. This can be attributed to the fact that, ISI system exhibits new sets of modes with considerable amount of mass participation in the higher modes.

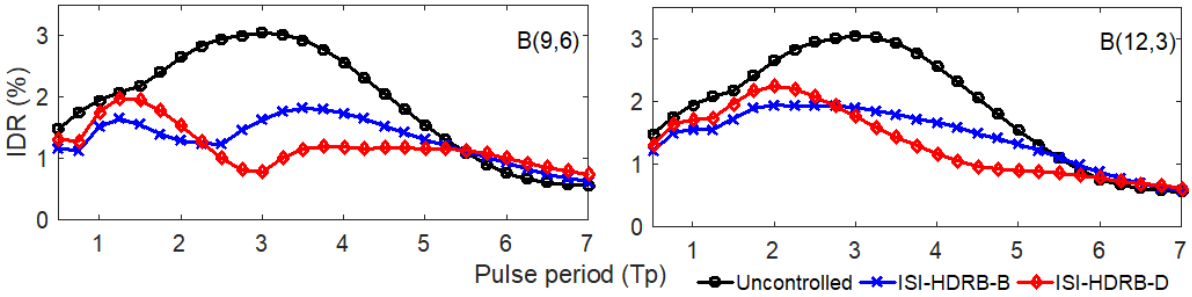

Figure 5 maximum variation of IDR (%) responses subjected to wide variety of pulse period.

8. Effect of structural non-linearity on MIDR (%) response of ISI system.

The influence of structural non-linearity on the IDR (%) response is shown in Figure 6. It may be observed that, if oscillatory character (γ) becomes 1.5, non-linear IDR (%) response for B(9,6) ISI system corresponds to fundamental modal period of the ISI structure is amplified compared to the linear counterpart. This implies that, IDR (%) response in a ISI system is underestimated by the linear model, as compared to the actual non-linear model.

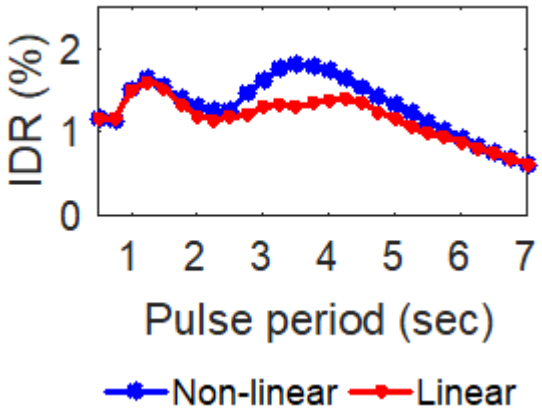

Figure 6 Effect of structural non-linearity on the B(9,6) ISI system

9. Conclusion

The present study attempt to investigate the seismic response behavior of the ISI frame subjected to the near fault pulse and non-pulse ground motions. Extensive numerical simulations are carried out by considering fifty near fault ground motions. The results of non-linear dynamic analysis highlighted that, seismic responses reduction (PFD, IDR and acceleration) efficiency is compromised under pulse ground motions. However, top floor acceleration response is much lower for the non-pulse motions as compared to the pulse motions. The characteristics of the pulse is strongly affect the IDR response. The ISI system shows two distinct peak (indicating resonance occurs) corresponds to the first and second modal period. It may be noted that, linear model of the ISI structure under predicts the IDR response in the vicinity of the fundamental mode.

10. References

[1] Saha A, Mishra S K (2019): Adaptive negative stiffness device based nonconventional tuned mass damper for seismic vibration control of tall buildings. *Soil dynamics and Earthquake Engineering*, 126.

[2] Ryan K L, Earl C L (2010): Analysis and design of inter-story isolation systems with nonlinear devices. *Journal of Earthquake Engineering*, 14.

[3] Ziyaeifar M, Noguchi H (1998): Partial mass isolation in tall building. *Earthquake Engineering and Structural Dynamics*,27.

[4] Charmpis D C, Komodromos P, Phocas M C (2012): Optimized earthquake response of multi-storey buildings with seismic isolation at various elevations. *Earthquake Engineering and Structural Dynamics*, 41.

[5] Reggio A, Angelis M D (2015): Optimal energy based seismic design of non-conventional tuned mass damper (TMD) implemented via inter-story isolation. *Earthquake Engineering and Structural Dynamics*, 44.

[6] Wang S J., Chang K C., Hwang J S., Lee B H (2011). Simplified analysis of mid-story seismically isolated buildings. *Earthquake Engineering and Structural Dynamics*, 40.

[7] Karavasilis T L, Bazeos N, Beskos D E (2007): Behavior factor for performance-based seismic design of plane steel moment resisting rrames. *Journal of Earthquake Engineering*, 11.

[8] EC 3 (1992). Eurocode 3, Design of Steel Structure, Part 1.1: General Rules for Buildings, European Prestandard ENV 1993-1-1/1992, *European Committee for Standardization (CEN)*, Brussels.

[9] EC 8 (2004). Eurocode 3, Design of Structures for earthquake resostance, Part 1: General Rules, Seismic actions and rules for Buildings, European Standard ENV 1998-1, Stage 51 Draft, *European Committee for Standardization (CEN)*, Brussels.

[10] FEMA 356 (2000). Pre-standard and commentary for the seismic rehabilitation of buildings. *Federal Emergency Management Agency Technical report*.

[11] Baker J. W (2007): Quantitative classification of near-fault ground motions using wavelet analysis. *Bulletin of the Seismological Society of Americ*a, 5(97).

[12] Tsopelas P C, Constantinou M C, Reinhorn A M (1994): 3D-BASIS-ME: Computer program for nonlinear dynamic analysis of seismically isolated single and multiple structures and liquid storage tanks, Technical report, *NCEER-94-0010*.

[13] SAP2000. *Structural software for analysis and design*.

[14] Mavroeidis G P, Papageorgiou A S (2003): A mathematical representation of near-fault ground motions. *Bulletin of Seismological Society of America*, 93(3).

